A dynamic network loading model for anisotropic and congested pedestrian flows

Flurin S. Hänseler*[a,b], William H.K. Lam[a], Michel Bierlaire[b], Gael Lederrey[b], Marija Nikolić[b]

[a] *Department of Civil and Environmental Engineering, The Hong Kong Polytechnic University, Hung Hom, Kowloon, Hong Kong, China*
[b] *Transport and Mobility Laboratory, School of Architecture, Civil and Environmental Engineering, École Polytechnique Fédérale de Lausanne, Switzerland*

Abstract

A macroscopic loading model for multi-directional, time-varying and congested pedestrian flows is proposed in this paper. Walkable space is represented by a network of streams that are each associated with an area in which they interact. To describe this interaction, a stream-based pedestrian fundamental diagram is used that relates density and walking speed in multi-directional flow. The proposed model is applied to two different case studies. The explicit modeling of anisotropy in walking speed is shown to significantly improve the ability of the model to reproduce empirically observed walking time distributions. Moreover, the obtained model parametrization is in excellent agreement with the literature.

Keywords: Pedestrian flow, network loading, macroscopic model, pedestrian fundamental diagram, anisotropy, calibration.

1. Introduction

There is a general need to better understand pedestrian traffic in densely populated areas such as airports, train stations, shopping malls or on busy pedestrian walkways. While particular applications like evacuation have received considerable attention (Helbing et al., 2002; Kirchner and Schadschneider, 2002), the simulation of general pedestrian flow is still insufficiently understood, in particular if multiple, potentially intersecting pedestrian 'streams' are involved.

*Corresponding author. Postal address: Transport and Mobility Laboratory, School of Architecture, Civil and Environmental Engineering, École Polytechnique Fédérale de Lausanne, Station 18, CH-1015 Lausanne, Switzerland.

Email addresses: flurin.haenseler@epfl.ch (Flurin S. Hänseler), william.lam@polyu.edu.hk (William H.K. Lam), michel.bierlaire@epfl.ch (Michel Bierlaire), gael.lederrey@epfl.ch (Gael Lederrey), marija.nikolic@epfl.ch (Marija Nikolić)

It can be broadly distinguished between microscopic and macroscopic modeling approaches. Microscopic models describe the movement of individual agents through space and time (e.g. Helbing and Molnár, 1995; Blue and Adler, 2001; Robin et al., 2009; Asano et al., 2010). They are relatively costly in their application and typically hard to calibrate (Hoogendoorn and Daamen, 2007). Macroscopic models consider traffic as a continuum, both as far as pedestrian movements and trip-maker decisions are concerned (e.g. Helbing, 1992; Hughes, 2002; Guo et al., 2011; Hoogendoorn et al., 2014). They are typically less accurate in describing complex crowd movements, such as they occur in congested or anisotropic flow. In return, their computation cost is independent of the number of pedestrians, which is beneficial for applications on large networks, for dynamic traffic assignment or for demand estimation (Abdelghany et al., 2012; Hänseler et al., 2015b).

In this paper, we present a macroscopic network loading model that explicitly takes anisotropy into account, i.e., the fact that the speed of pedestrians may differ depending on their walking direction. This has not been achieved at the macroscopic level so far, at least for the case of general multi-directional flow. We note that Jiang et al. (2009) consider an anisotropic model which however is only capable of describing bi-directional flow. Besides, there is a range of macroscopic models considering 'multi-directional' flow, but no anisotropy (Hughes, 2002; Guo et al., 2011; Hänseler et al., 2014). In the remainder of this paper, we first review the relevant body of literature on macroscopic modeling and empirical characterization of multi-directional pedestrian flow. We then propose an anisotropic loading model for pedestrians flows. The proposed model is calibrated on real data and applied to two real case studies.

2. Literature review

Among the macroscopic approaches for modeling pedestrian flows, we focus on continuum models, and on related phenomenological models. The review is not meant to be exhaustive, but rather to provide the necessary context for the modeling framework presented in Section 3. For a comprehensive review of pedestrian flow models including microscopic and hybrid models, we refer to Duives et al. (2013).

Continuum models interpret pedestrians as particles of flow that are conserved. They formulate a set of partial differential equations (PDEs) in which walking speed is typically determined by a fundamental diagram relating pedestrian density and speed. Inspired by the kinematic wave theory, it is assumed that the fundamental diagram also holds for non-stationary traffic, implying that pedestrians adapt their speed instantaneously with infinite acceleration.

One of the first continuum models for pedestrian movements has been proposed by Al-Gadhi and Mahmassani (1990), who study circular movements around religious stone monuments during the Hajj, a Muslim pilgrimage to Makkah, Saudi Arabia. Their approach has been generalized by Hughes (2002) in his seminal 'continuum theory for the flow of pedestrians.' This theory is a two-dimensional extension of the Lighthill–Whitham–Richard (LWR) model that is used to approximate the traffic movement on a

uni-directional highway (Lighthill and Whitham, 1955; Richards, 1956). Hughes' continuum theory allows for multi-commodity flow involving pedestrians with different walking directions and destinations.

Huang et al. (2009) show that the pedestrian route choice strategy in Hughes' model satisfies the reactive dynamic user equilibrium. A numerical procedure to solve the coupled system of PDEs is presented and applied to a numerical example. Jiang et al. (2009) extend this approach by adopting a bi-directional density-speed relationship that can be used to simulate two groups of pedestrians traveling on crossing paths. The emergence of lanes and stripes is reported. Such phenomena of self-organization had already been observed previously in a similar model by Treuille et al. (2006), as well as later by Colombo et al. (2012) who study pattern formation from a mathematical point of view.

Hoogendoorn et al. (2014, 2015) derive a continuum model from a microscopic pedestrian model. As for the previous models, pedestrian flow is assumed in equilibrium by setting all acceleration terms to zero. A closed-form expression for the walking speed is obtained by approximating the density using a first-order Taylor series expansion. The model is then specified such that a linear and isotropic density-speed relationship results. Several numerical examples are considered using a two-dimensional Godunov scheme (Lebacque, 1996; van Wageningen-Kessels et al., 2015a).

There are several further macroscopic continuum models that are noteworthy. Inspired by classical fluid dynamics, Bellomo and Dogbé (2008) study the motion of pedestrians by describing a system of two PDEs invoking the conservation of mass and the balance of linear momentum. Piccoli and Tosin (2011) present a measure-based model, in which a family of measures are pushed forward by some flow maps, providing an estimate of the space occupation of pedestrians at successive times. Schwandt et al. (2013) use a multiphase approach based on a convection-diffusion equation and apply it to a cross-flow experiment. Recently, Degond et al. (2013) have derived a continuum model from a vision-based agent model (Ondřej et al., 2010), and Degond and Hua (2013) study a hydrodynamic model of self-organized dynamics that is inspired from interactions of animals observed in nature.

The above models have in common that they express a system of PDEs that are solved numerically by discretization. The resulting solution schemes are similar to a group of models that are referred to as 'phenomenological.' Phenomenological models may provide a comparable level of detail in terms of spatial and temporal dynamics, but they are not a direct product of the discretization of a system of PDEs. Having said that, they lend many ideas from such discretization schemes, in particular the cell transmission model (CTM, Daganzo, 1994, 1995). Phenomenological models leave more freedom to the modeler and are sometimes more accurate, as the systems of PDEs discussed previously do not represent any physical law in the first place. Furthermore, they are typically less costly to apply in practice. In fact, with the exception of Al-Gadhi and Mahmassani (1990), none of the above approaches have been calibrated on a real case study.

Asano et al. (2007) have been first to propose a generalized CTM to describe pedestrian flows. As used by Daganzo in the context of vehicular traffic, an isotropic trape-

zoidal fundamental diagram is assumed in their pedestrian cell transmission model. No framework for estimating 'turning proportions' is provided. Instead, the fractions of pedestrians associated with each walking direction are exogenously given, and the exact sequence of cells that a pedestrian traverses must be known in advance. This can be a severe constraint for the application of their model in practice.

Extended by a discrete potential field, Guo et al. (2011) present a related framework to study pedestrian route choice behavior and congestion during evacuation. A specification of the exact sequence of cells for pedestrians is no longer required. However, their framework is only capable of dealing with a trapezoidal fundamental diagram, which is shown for the case of uni-directional flow. The use of a more general density-flow relationship, as it may be found in applications different from evacuation, is not possible.

In a recent study, we have undertaken such an extension (Hänseler et al., 2014). The proposed formulation allows for a general, non-linear pedestrian density-flow relationship, which however needs to be isotropic. The concept of a cell-based potential field is adapted, and combined with a logit-type en-route path choice model. It is shown that, depending on the specification of the pedestrian model, various types of bottleneck behavior ranging from disciplined queueing to impatient 'jostling' can be reproduced.

The large majority of macroscopic pedestrian models mentioned thus far rely on isotropic density-speed relationships. Only Al-Gadhi and Mahmassani (1990) and Jiang et al. (2009) consider a bi-directional fundamental diagram for two specific applications. Yet pedestrian flow is in many cases multi-directional and, in particular under congested conditions, anisotropic. Anisotropy is the property of being direction-dependent, here of the walking speed. In anisotropic pedestrian flow, the walking speed at the same point in space may be different depending on the orientation of a pedestrian. This definition is consistent with that used in material science or physics (e.g. Sayir et al., 2008). For an alternative definition of anisotropy in the context of microscopic models, see e.g. Hoogendoorn and Bovy (2002).

In the following, some findings from empirical pedestrian research are recapitulated, which are then used to construct a dynamic network loading model that can describe multi-directional, anisotropic and congested pedestrian flows. This has been achieved only at the microscopic level so far.

Several empirical studies consider a 'stream'-based interpretation of flow to construct an anisotropic pedestrian density-speed relationship. In these studies, multi-directional pedestrian flow is decomposed into a set of uni-directional streams that interact within the same space (Nikolić and Bierlaire, 2014). The direction of these streams depends on the type of walking facilities and may be known a priori, or inferred from available data.

One of the earliest studies investigating anisotropy in pedestrian flow is due to Navin and Wheeler (1969). They observe that counter-flow reduces walking speed, with a maximum reduction of about 14.5% in case of a flow ratio of 10% : 90%, and a minimal reduction of about 4% in case of symmetric flow. This is in qualitative agreement with findings by Lam et al. (2002) who report that the maximum reduction in capacity is around 19% for the same 10% : 90% split ratio.

Several researchers calibrate anisotropic density-speed relationships for pedestrian

counter-flow, some of the earliest being Al-Gadhi et al. (2002). These relationships have in common that the speed of a group of pedestrians moving in one direction depends on the density of each of the two opposing streams. Zhang et al. (2012) provide a review of more than two decades of research on bi-directional pedestrian fundamental diagrams. While it seems widely acknowledged that the minor flow is slower than the major one, they conclude that no commonly accepted model formulation for bi-directional pedestrian fundamental diagram exists yet. Based on their own experiments, they find that anisotropy becomes apparent for densities beyond $1\,\mathrm{ped/m^2}$, and that the maximum specific flow in uni-directional streams is significantly larger than that in a bi-directional setting.

In a later study, Zhang and Seyfried (2014) extend their experiments to include cross-flow, i.e., bi-directional pedestrian flow with an orthogonal intersection angle. They find little difference in the shape of the pedestrian fundamental diagram between counter- and cross-flow and hypothesize that the anisotropic effects reducing the walking speed are independent of the intersection angle.

These results are in contrast with the findings by Wong et al. (2010) who experimentally investigate the bi-directional pedestrian flow with intersection angles of 45°, 90°, 135° and 180°. They find that the conflicting effect maximizes for a head-on situation with a 180°-intersection angle. Based on their experimental results, they propose a bi-directional pedestrian density-speed relationship that considers the stream densities and intersection angle. In a related study, Xie and Wong (2015) generalize that approach to a n-directional pedestrian stream model, i.e., a pedestrian fundamental diagram that explicitly considers the joint presence of n uni-directional streams.

Empirical observations show that it is often problematic to relate a single speed to each density level in pedestrian flow. Nikolić et al. (2016) consider probabilistic formulations of an isotropic density-speed relationship to relax this assumption. Depending on factors such as the local flow pattern, trip purpose, age and gender, different pedestrians may walk slowly or run fast under the same conditions. In the context of macroscopic models, a density-speed relationship is primarily used to approach the expected speed at a given density. Thus, deterministic formulations are sufficient for the remainder of this work.

A typical phenomenon of multi-directional pedestrian flow is the formation of patterns of self-organization (Helbing et al., 2005). Self-organization, such as the dynamic formation of lanes, leads to more efficient behavior when pedestrians walk in different directions (Moussaïd et al., 2010). Pedestrian fundamental diagrams can capture these patterns only implicitly (see e.g. Zhang et al., 2012). The explicit modeling of phenomena of self-organization at both the microscopic and macroscopic level is already discussed widely in the literature (Helbing and Molnár, 1995; Treuille et al., 2006; Jiang et al., 2009; Hoogendoorn et al., 2014).

In this paper, we aim to overcome the assumption of isotropy adopted in macroscopic pedestrian models by developing a dynamic network loading model that relies on a stream-based formulation of a pedestrian fundamental diagram. The proposed model is motivated by Hughes' continuum theory and recent research focusing on the empiri-

cal characterization of multi-directional pedestrian flow. The mathematical formulation is based on a heuristic, multi-directional discretization scheme that is related to the cell transmission model. Besides the explicit consideration of anisotropy, the model is designed to be easily applicable to large and complex real-world applications. A Java implementation and several illustrative test cases are available on GitHub (Hänseler and Lederrey, 2015).

3. Model framework

We consider a discrete-time discrete-space model where each time interval $\tau \in \mathcal{T}$ is of uniform length Δt. As suggested by Løvås (1994), walkable space is represented by a directed graph $\mathcal{G} = (\mathcal{N}, \Lambda)$, where $\mathcal{N}$ represents the set of nodes $\nu \in \mathcal{N}$, and Λ the set of directed streams $\lambda \in \Lambda$. Nodes through which pedestrian traffic is discharged and leaves the network are referred to as origin/destination nodes, and their set is denoted by $\mathcal{N}_{OD} \subseteq \mathcal{N}$. While their typical position is at the border of a walking facility, OD nodes can also be located in the interior if they represent an access way to e.g. an elevator or an escalator. Nodes have no physical length.

A stream λ connects two nodes and has a fixed length $L_\lambda > 0$. It carries pedestrians only in one direction. Streams are obtained by decomposing the generally multi-directional flow. This decomposition depends on the prevalent pedestrian flow, and the geometry of the walking facility. It is assumed that a meaningful decomposition is known a priori. In the literature on empirical flow characterization, several decomposition strategies are discussed (Nikolić and Bierlaire, 2014; Xie and Wong, 2015).

Walkable space is furthermore partitioned into a set of areas $\mathcal{X}$. Every stream λ is associated with an area $\xi \in \mathcal{X}$, defining a space in which it interacts with other streams. The surface size of an area ξ is denoted by A_ξ, which takes into account a potential presence of internal obstacles. Such obstacles include any object that reduces the walkable space, such as a pillar or a trash bin. No prior assumptions about the shape and size of areas are necessary. The set of streams associated with area ξ is denoted by Λ_ξ, with $\Lambda_\xi \subset \Lambda$ and $\Lambda_\xi \cap \Lambda_{\xi'} = \emptyset$ if $\xi \neq \xi'$.

Fig. 1 illustrates the proposed space representation at the example of a longitudinal corridor with an orthogonal space discretization. In this illustration, multi-directional flow is decomposed into left-right as well as diagonal movements, resulting in six distinct flow directions. Areas are delimited by solid lines, streams represented by dashed lines, and nodes by circles. Since streams are direction-specific, each dashed line in Fig. 1 represents two streams, one in each direction. Pedestrians may cross from one area to another at any position along the joint boundary, and not only through nodes. Likewise, when traversing areas, pedestrians are not confined to the dashed lines, which only represent their direction of flow conceptually. Origin/destination nodes at both ends of the corridor are represented by the two stars.

An orthogonal discretization as in Fig. 1 represents the most common specification for flow models relying on a fundamental diagram (Treuille et al., 2006; Huang et al., 2009). The size of areas is typically between 1 m^2 and 10 m^2. In this range, the model

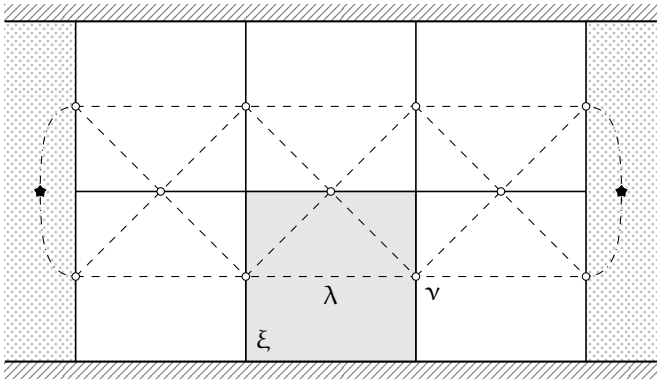

Figure 1: Illustration of space representation.

dynamics are found to be approximately scale-invariant. Specifically, we have tested several discretization meshes in that range at the example of the case studies presented later, with no significant changes in the resulting model dynamics and calibration parameters. For artificial test scenarios with abrupt changes in demand and density, this result may however not hold. The main alternatives to an orthogonal space discretization are triangular or hexagonal grids (Guo et al., 2011; Chen et al., 2014; van Wageningen-Kessels et al., 2015b). Even irregular discretization geometries may be envisaged if they better fit the infrastructural layout.

A route ρ is defined by a pair of origin and destination nodes (ν_o^ρ, ν_d^ρ), $\nu_o^\rho, \nu_d^\rho \in \mathcal{N}_{OD}$, and a set of streams Λ_ρ that connect them. The set Λ_ρ may be obtained by selecting streams individually, or by including all streams that are associated with a set of areas. There can be several routes connecting the same pair of OD nodes. Each route starts and ends at an OD node, but cannot contain any OD node in between. The set of all routes is denoted by $\mathcal{R}$.

Depending on the network $\mathcal{G}$ and the set of streams Λ_ρ, multiple 'stream sequences' may connect the origin and destination of a route ρ. Such stream sequences are referred to as paths. To avoid their explicit enumeration, the concept of a path is not explicitly used. Instead, the choice of a path within a route is considered by means of turning proportions that are computed at every node. They may depend both on the route and the prevailing traffic conditions. Depending on their specification, pedestrians may be distributed across multiple paths within a route, or stick to a single one, for instance the shortest path.

Pedestrians are organized in 'packets.' A pedestrian packet ℓ is characterized by a route ρ_ℓ, a departure time interval τ_ℓ, and the number of people X_ℓ that it contains. The set of all packets is denoted by $\mathcal{L} \subset \mathcal{R} \times \mathcal{T}$. The size X_ℓ of each pedestrian packet $\ell \in \mathcal{L}$ is assumed to be known a priori, and the corresponding demand vector is denoted by $\mathbf{X} = [X_\ell]$. Such information can be inferred from a demand estimation framework in combination with a suitable route choice model, which are readily found in the literature (Cascetta et al., 1993; Hoogendoorn and Bovy, 2004; Hänseler et al., 2015b).

A conservation principle with respect to the number of pedestrians on each stream is combined with an empirical density-speed relationship for calculating the flows between them. Within a stream, pedestrians are assumed to be homogeneously distributed, and their movements are not modeled explicitly. Moreover, pedestrians are assumed to be homogeneous with respect to their walking characteristics. An extension to multi-commodity flow is in principle possible (see e.g. Cooper, 2014), but out of the scope of this work.

When pedestrian packets are propagated along the streams, they disperse by splitting up into 'fragments.' In principle, pedestrian packets can split indefinitely, but they merge again such that there is at most one fragment per packet in a stream. From a practical view point, dispersion can be seen as mimicking the presence of slow and fast pedestrians. This is an interesting property for traffic assignment, where estimates of walking time distributions are more useful than simple point estimates.

The state of the model at any time interval is described by the distribution of the fragments on the network. The number of pedestrians associated with packet ℓ in stream λ during time interval τ is denoted by $M^{\ell}_{\lambda,\tau}$ and referred to as the corresponding 'fragment size.' The sum of all fragments in a stream λ during time interval τ is denoted by $M_{\lambda,\tau}$ and referred to as the stream accumulation. The vector of stream accumulations associated with area ξ and time interval τ is denoted by $\mathbf{M}_{\xi,\tau} = [M_{\lambda,\tau}]$, with $\lambda \in \Lambda_{\xi}$.

Similarly, each stream λ during time interval τ is associated with a walking speed $v_{\lambda,\tau}$, which is grouped with the other stream speeds of the same area ξ in the velocity vector $\mathbf{v}_{\xi,\tau} = [v_{\lambda,\tau}]$, $\lambda \in \Lambda_{\xi}$. It is assumed that a functional relationship between the stream accumulation and velocity vectors for each area ξ and time interval τ exists. If v_f represents the 'global' free-flow walking speed, the stream velocity vector associated with area ξ during time interval τ can be accordingly expressed as

$$\mathbf{v}_{\xi,\tau} = v_f \mathbf{F}_{\xi,\tau}(\mathbf{M}_{\xi,\tau}), \tag{1}$$

where $\mathbf{F}_{\xi,\tau}(\mathbf{M}_{\xi,\tau})$ represents the corresponding dimensionless density-speed relationship. Eq. (1) describes the relationship between the accumulation of each stream in an area, and the corresponding pedestrian stream speeds. Several possible specifications, both isotropic and anisotropic, are provided in Section 4. Note that in practice, mostly time-invariant specifications are used due to the difficulty of calibrating time-dependent models. The former are typically referred to as pedestrian fundamental diagrams.

Eq. (1) implies that pedestrians instantaneously adapt their speed if a change in accumulation occurs. In traffic flow theory, this is characteristic for first-order flow models. For pedestrian models, such an assumption is particularly well suited, since pedestrians can accelerate from standstill to free-flow walking speed almost immediately and vice versa (Weidmann, 1992).

Regarding the functional form of the vectorial density-speed relationship $\mathbf{F}_{\xi,\tau}(\mathbf{M}_{\xi,\tau})$, two assumptions are made. These are inspired by Hughes' continuum theory for pedestrian flows (Hughes, 2002).

First, it is hypothesized that in an unoccupied area, the walking speed in every stream must be larger than zero, but may not exceed the global free-flow speed. If $F_{\lambda,\tau}$

represents the entry in $\mathbf{F}_{\xi,\tau}$ associated with stream $\lambda \in \Lambda_\xi$, this translates to

$$0 < F_{\lambda,\tau}(\mathbf{0}) \leq 1 \ \forall \ \lambda \in \Lambda_\xi, \xi \in \mathcal{X}, \tau \in \mathcal{T}, \tag{2}$$

where $\mathbf{0}$ represents the null vector of length $|\Lambda_\xi|$. The walking speed at zero density can be lower than the global free-flow speed, which may be adequate for instance in uneven terrain. It may however not be zero, excluding phenomena like waiting. The resulting formulation therefore represents an exclusive walking model like most macroscopic approaches in the literature.

Second, walking speed is assumed not to increase with increasing stream accumulation, i.e.,

$$\frac{\partial F_{\lambda,\tau}}{\partial M_{\lambda',\tau}} \leq 0 \ \forall \ \lambda, \lambda' \in \Lambda_\xi, \xi \in \mathcal{X}, \tau \in \mathcal{T}. \tag{3}$$

For univariate density-speed relationships such as most isotropic fundamental diagrams, Eq. (3) corresponds to the assumption of monotonicity. It is widely accepted under 'normal' conditions (Daganzo, 1994; Hughes, 2002), and required to guarantee the uniqueness of a critical accumulation and speed, which is important for the envisaged model.

Some fundamental diagrams specify a jam density k_{jam}, i.e., a density at which all pedestrian movement halts. Equivalently, at the area level, a storage capacity $N_\xi^{jam} = k_{jam} A_\xi$ may be considered, representing the maximum number of pedestrians that can be present in an area at any time. In that case, it is further required that

$$F_{\lambda,\tau}(\mathbf{M}_{\xi,\tau}) = 0 \text{ if } N_{\xi,\tau} = N_\xi^{jam}, \tag{4}$$

where $N_{\xi,\tau} = \sum_{\lambda \in \Lambda_\xi} M_{\lambda,\tau}$ denotes the total accumulation in area ξ during time interval τ.

To propagate pedestrians from one stream to the next, route-specific turning proportions at each node need to be known. They may be exogenous, or computed by an en-route path choice model based on the prevailing pedestrian traffic conditions. Assuming that pedestrians associated with the same route follow the same en-route path choice behavior, the turning proportion corresponding to the stream sequence $\lambda \rightarrow \lambda'$ for the ensemble of people following route ρ that are in stream λ during time interval τ may be denoted by $\delta^\rho_{\lambda \rightarrow \lambda',\tau}$. Since pedestrians can only be sent to adjacent streams that are part of their route, it must hold that

$$\sum_{\lambda' \in \Theta^\rho_\lambda} \delta^\rho_{\lambda \rightarrow \lambda',\tau} = 1, \tag{5}$$

where Θ^ρ_λ denotes the set of streams that originate from the end of stream λ and are part of route ρ. Typically, a potential field is assumed to exist from which the turning proportions for local path choice can be inferred (Hughes, 2002; Guo et al., 2011). These turning proportions guide the pedestrians along their route to their desired destination, taking the prevailing pedestrian traffic conditions into account. Depending on their specification, the en-route path choice may resemble a diffusion model, a shortest path model, or a mixture of both. In Section 4, a specification is provided that can reproduce such walking behavior.

Finally, the time discretization has to be such that pedestrians cannot traverse more than one stream in a single time step. In numerical mathematics, this consideration is referred to as the Courant–Friedrichs–Lewy (CFL) condition (Courant et al., 1967). It can be expressed as

$$\Delta t \leq \frac{L_\lambda}{v_f}, \ \forall \lambda \in \Lambda. \tag{6}$$

According to Eq. (6), the ratio of the shortest stream length and the free-flow walking speed represents an upper bound for the time discretization. For instance, for the space representation shown in Fig. 1, the constraining length is that of the diagonal streams, which are shorter than the horizontal ones.

The actual choice of the time step Δt is not critical for the stability of the model, but known to have an influence on numerical dispersion and computational cost (van Wageningen-Kessels et al., 2015a). In practice, it has been observed that such dispersion can even lead to more realistic results (Lebacque, 1996). As such, the time step can be seen as a calibration parameter. In this work, this possibility is not explored, and as in most traffic flow studies, the bound defined in Eq. (6) is used to specify the time step, i.e.,

$$\Delta t = \min_{\lambda \in \Lambda} \{L_\lambda / v_f\}. \tag{7}$$

Based on the above representation of pedestrians, walking space and time, as well as the notion of a density-speed relationship and a conservation principle, a pedestrian network loading model can be defined. The corresponding approach is inspired by Daganzo's cell transmission model and a recent adaptation to pedestrian flows (Daganzo, 1994; Hänseler et al., 2014). Details of the numerical scheme may be found in Appendix A.

Conceptually, sending capacities are computed for each pedestrian fragment at every time step. Simultaneously, for every stream and area, receiving capacities are computed. Taking these capacity constraints into account, transition flows between streams may be obtained. A 'demand-proportional supply distribution' is thereby assumed, i.e., no distinction in the distribution of supply capacity with respect to specific directions is made (Asano et al., 2007). In principle, other supply distribution schemes may be envisaged. A variety of related models have been proposed in the literature dealing with multi-legged junctions in road networks (Daganzo, 1995; Lebacque, 1996; Jin and Zhang, 2003). Most of these approaches are however specific to the case of vehicular traffic, and not directly applicable in the context of pedestrian flows.

The resulting modeling framework represents a significant improvement over the aforementioned pedestrian cell transmission model by Hänseler et al. (2014). In that study, multi-directional pedestrian flow is approximated by an 'equivalent' uni-directional flow with the same overall density, where the directionality of flow is entirely ignored. Here, instead an explicit decomposition of flow into pedestrian streams is made, of which each is associated with a distinct direction, density and speed. The concept of 'cells' is replaced by that of 'streams,' which interact within 'areas.' To describe this interaction, an anisotropic density-speed relationship can be used, whereas the previous approach

only allows for isotropic formulations. This represents a critical improvement when describing multi-directional flows under congested conditions. While an isotropic approach may be sufficient for modeling uni-directional flow or flow in absence of congestion, it does not suffice for describing congested, multi-directional flow. Such flow conditions are however increasingly found in railway stations, urban areas, or stadiums, representing important fields of application of pedestrian network loading models for e.g. planning purposes, demand estimation, or crowd management.

To apply the proposed model in practice, four types of exogenous inputs are required. These are (i) the route flow demand in the form of the set of pedestrian packets $\mathcal{L}$, (ii) a network representation in the form of the set of streams Λ and their associated areas $\mathcal{X}$, (iii) a density-speed relationship such as an anisotropic fundamental diagram, and (iv) an en-route path choice model that provides the turning proportions at nodes. The first may be obtained by a demand estimation model, or by direct observation. The second is given by the infrastructure of interest. The third and fourth input are discussed in the following section.

4. Model specification and calibration

A specification of the stream-based pedestrian density-speed relationship and the turning proportions is provided in the following. To assess the comparative advantage of an anisotropic density-speed relationship, additional isotropic specifications are considered.

4.1. Density-speed relationship

To demonstrate the anisotropic features of the model, we propose a stream-based pedestrian fundamental diagram (SbFD). It represents a generalization of the formulation by Wong et al. (2010) to multiple streams that interact in a pair-wise manner as described by Xie and Wong (2015). We however do not directly use Xie and Wong's approach, as it requires solving a fixed-point problem, for which the existence and uniqueness of a solution are not a priori guaranteed. The specification is a means to explore the walking behavior in the network loading model, and not the main focus of this research.

Let $\phi_{\lambda,\lambda'}$ denote the intersection angle between streams λ and λ' with $\phi_{\lambda,\lambda'} = 0$ if $\lambda = \lambda'$, and let β and ϑ denote model parameters. We assume that the walking speed of stream $\lambda \in \Lambda_\xi$ is given by

$$v_\lambda = v_f \exp\left(-\vartheta\left(\frac{N_\xi}{A_\xi}\right)^2\right) \prod_{\lambda' \in \Lambda_\xi} \exp\left(-\beta(1-\cos\phi_{\lambda,\lambda'})\frac{M_{\lambda'}}{A_\xi}\right). \tag{8}$$

Eq. (8) represents a generalization of Drake's one-dimensional traffic model (Drake et al., 1967). The first exponential term considers the isotropic reduction in walking speed induced by the overall accumulation in an area. A large value of ϑ implies a strong reduction in walking speed with increasing accumulation, and vice versa. The second term, i.e., the product of exponentials, represents the combined reduction in walking

speed due to 'friction' with other pedestrian streams, depending on their density and the intersection angle. Similarly, a large value of β increases the magnitude of these anisotropic conflicting effects. In Appendix B, some properties of Eq. (8) are discussed, and further explanation for the choice of the specification is provided.

Wong et al. (2010) estimate v_f at 1.034 m/s and ϑ at 0.075 m^4, and Xie and Wong (2015) at 1.070 m/s and 0.065 m^4, respectively. For β, no parameter estimates are available in the literature. If it is set to zero, Drake's isotropic fundamental diagram,

$$v_\lambda = v_f \exp\left(-\vartheta\left(\frac{N_\xi}{A_\xi}\right)^2\right), \tag{9}$$

results.

For a rectangular space discretization, multi-directional flow is generally decomposed in 12 uni-directional streams connecting each pair of area edges. There are eight distinct directions to cross an area, namely left/right, up/down, and diagonally. In the subsequent case studies, accordingly there are up to eight directions of flow and up to 12 streams per area (see Fig. 3b).

We note that other, more advanced anisotropic formulations of pedestrian fundamental diagrams can be envisaged. In multi-directional pedestrian flow, different behavioral regimes are likely to exist. For instance, for the major stream, a leader-follower behavior may be predominant, while for the minor stream, collision avoidance is more important. Both of these mechanisms probably depend differently on the intersection angle. A case distinction for acute, right and obtuse angles may be beneficial. The exploration of such advanced specifications is left for future research.

In terms of isotropic pedestrian density-speed relationships, one of the most widely used specifications is that of Weidmann (1992), who defines the isotropic walking speed of any stream λ in area ξ as

$$v_\lambda = v_f \left\{1 - \exp\left[-\gamma\left(\frac{A_\xi}{N_\xi} - \frac{1}{k_{jam}}\right)\right]\right\}. \tag{10}$$

According to Weidmann (1992), the free-flow walking speed is estimated at $v_f = 1.34$ m/s, the shape parameter at $\gamma = 1.913\,m^{-2}$, and the jam density at $k_{jam} = 5.4\,m^{-2}$. Specification (10) has been obtained from a literature review, trying to describe different settings using a single relationship. As such, it may not be the most realistic fundamental diagram for any specific flow configuration, but one that is comparably general and applicable in absence of anisotropy.

Finally, as a benchmark for the assessment of the various formulations, a 'zero-model' is considered, where the walking speed is constant over space and time and given by

$$v_\lambda = v_f. \tag{11}$$

Further information related to these density-speed relationships, in particular including a derivation of critical densities, is provided by Hänseler (2016).

4.2. Turning proportions

It is assumed that a potential field exists from which local turning proportions at each node can be inferred (Hughes, 2002; Guo et al., 2011). These turning proportions are traffic-dependent and route-specific. Each node ν is assigned a potential $P^{\rho}_{\nu,\tau}$ representing the remaining walking time along the fastest path on route ρ at traffic conditions as they are prevalent during time interval τ. The potential $P^{\rho}_{\nu,\tau}$ can be calculated using any shortest path algorithm (Dijkstra, 1959). For any node ν that is not associated with route ρ, it is set to infinity.

In principle, various specifications including a linear attribution scheme may be used to deduce turning proportions from node potentials. In the context of discrete choice theory (Ben-Akiva and Lerman, 1985), the potential of a node may be interpreted as its 'utility.' Using a logit-type model with weight μ, the turning proportion associated with the stream sequence $\lambda \rightarrow \lambda'$ and route ρ during time interval τ, with $\lambda' \in \Theta^{\rho}_{\lambda}$ and ν the joint node of streams λ and λ', can be calculated by

$$\delta^{\rho}_{\lambda\rightarrow\lambda',\tau} = \frac{\exp\left(-\mu P^{\rho}_{\nu^{d}_{\lambda'},\tau}\right)}{\sum_{\lambda''\in O^{\rho}_{\nu}} \exp\left(-\mu P^{\rho}_{\nu^{d}_{\lambda''},\tau}\right)}, \tag{12}$$

where the set of streams emanating from node $\nu \in \mathcal{N}$ associated with route ρ is denoted by O^{ρ}_{ν}. This specification is memory-less in that the choice of the next stream λ' depends only on the current node, but not on the previous stream λ. This property can be exploited to reduce the cost of computing these fractions.

Moreover, specification (12) assumes that pedestrians rely solely on instantaneous information to make their path-choice decisions. No predictive information is available to them, and travel cost to the respective destination is minimized in a reactive manner (Hoogendoorn and Bovy, 2004).

In the literature, several related methods have been proposed to generate potential fields, and to derive turning proportions from them (Hughes, 2002; Treuille et al., 2006; Guo et al., 2011; Hänseler et al., 2014). The concept as such is rather well established, and a large diversity of approaches exist. The latter is due to the complexity of pedestrian route/path choice, which is influenced by various factors such as ambient conditions, travel purpose, signage, habit or physical effort. Data availability is generally limited, making an accurate modeling of these relationships difficult. In fact, neither Hughes (2002) nor Guo et al. (2011) use real data to calibrate their model, and parameter identifiability can be a problem (Hänseler et al., 2014). We leave the development of more detailed models for future research.

4.3. Calibration

A pseudo maximum likelihood framework is used to calibrate the model (Besag, 1975; Gourieroux et al., 1984). The calibration is based on walking times, which are comparatively easy to observe, yield a robust parametrization, and are an important output of a network loading model. Previously, we have also investigated the use of

other calibration measures, such as density and local flows, or a combination thereof (Hänseler et al., 2014). The results have shown that a calibration based on walking times alone yields an accurate parametrization, and greatly simplifies the estimation process as compared to a multi-objective optimization problem. Besides, for some of the case studies analyzed in the following, only demand and walking time data are available anyway.

In the following, it is assumed that for each pedestrian i, the route ρ_i, the departure time t_i^{dep} and the walking time tt_i are known by observation without measurement error. The observed walking time tt_i^{obs} of pedestrian i is considered as a draw from a random variable TT_i^{obs}, whose distribution f_i^{obs} is unknown. In practice, knowledge of that distribution is not available, except if the same experiment is run multiple times (Kretz et al., 2006).

Let $f_i^{est}(tt|\mathbf{X}, \theta)$ denote the walking time probability density of pedestrian i that is generated by the model for a demand $\mathbf{X}$ and a set of parameters θ. It is given by the walking time distribution of the corresponding pedestrian packet $\ell(i)$, with $t_i^{dep} \in \tau_\ell$ and $\rho_i = \rho_\ell$.

The pseudo log-likelihood to reproduce the walking time vector $\mathbf{tt}_{obs} = [tt_i^{obs}]$ for a sample of n pedestrians can then be expressed as

$$\widetilde{\mathcal{L}}(\mathbf{tt}_{obs}|\mathbf{X}, \theta) = \sum_{i=1}^{n} \log\left(f_i^{est}(tt_i^{obs}|\mathbf{X}, \theta)\right). \tag{13}$$

The objective of the calibration is to find a parametrization θ such that the pseudo likelihood of reproducing the observed walking times is maximized, i.e.,

$$\widehat{\theta} = \arg\max \widetilde{\mathcal{L}}(\mathbf{tt}_{obs}|\mathbf{X}, \theta). \tag{14}$$

Eq. (14) is referred to as the pseudo maximum likelihood estimator. It differs from the actual maximum likelihood estimator in that any correlation between measurements is neglected. There are generally two sources of correlation, namely serial and spatial. Serial correlation is mostly an issue if multiple measurements of the same pedestrian are considered. This is not the case here, since only one walking time estimate per person is available. Spatial correlation occurs if observations are dependent across pedestrians. Such clustering is indeed present in that several pedestrians may be associated with the same pedestrian packet, and thus be described by the same estimated walking time distribution. This leads to an artificial weighting of these distribution terms, which the pseudo likelihood does not account for.

With decreasing packet sizes, the clustering effect vanishes. By changing the space discretization, the time discretization changes through Eq. (7), and indirectly the packet sizes can be influenced. In the case studies described in the next section, the discretization is such that a large majority of packets contain at most two or three pedestrians, and are of similar size. We have tested different discretizations and found only a very small influence on the estimates (Lederrey, 2015). At least if packets are small, the role of spatial correlation seems to be negligible, and the maximization of the pseudo likelihood

defined in Eq. (13) provides a consistent estimate of the parameters. If large packets are present, other estimation techniques such as indirect inference may be more appropriate (Gourieroux et al., 1993).

Even if it is unbiased, the pseudo likelihood estimator is less efficient than the actual maximum likelihood estimator. Standard techniques for statistical inference need in principle to be adapted for use in a pseudo likelihood setting. Specifically, the Cramér-Rao bound is generally not reached, and the standard likelihood-ratio test does not apply, as the asymptotic distribution of the differences in pseudo log-likelihoods is not χ^2-distributed (Dodge, 2006). Following Hoogendoorn and Daamen (2007), and taking into account the negligible role of clustering in the considered case studies, we still provide standard variance estimates. We note however that their significance in a pseudo likelihood framework is limited, and refer to the literature for generalized approaches that should be used if pedestrian packets are large (Bai, 1999; Moreira, 2003). To assess the goodness-of-fit of a specification, the Akaike information criterion (AIC) based on the pseudo likelihood is reported. We have also computed the Bayesian information criterion (BIC), and found that it agrees with the AIC on the preferred model for each of the studied cases.

The estimator defined by Eq. (14) represents an improvement notably over the calibration routine used by Hänseler et al. (2014). In that study, a least squares approach based on mean walking times has been employed. The newly proposed method is superior in that it is statistically more rigorous and computationally more efficient.

To solve Eq. (14), a derivative-free trust-region method for constrained optimization in combination with random sampling of initial parameters is used (Powell, 2009). Other globally convergent optimization methods such as simulated annealing or evolutionary algorithms yield the same results, but turn out to be slower. Derivative-based optimization methods are not recommended, as no derivative information of Eq. (14) is available.

5. Case studies

Two case studies are considered, one based on a set of pedestrian counter-flow experiments conducted in Hong Kong, China, and one based on a pedestrian cross-flow experiment in Berlin, Germany. The first is particularly useful in that it explores a large range of pedestrian traffic conditions, and the second in that it considers the walking behavior of a typical student population in their daily environment. From a methodological point of view, the first case study allows to investigate aspects such as model performance, robustness and predictive power, and the second case study is useful for obtaining a concrete specification applicable to real case studies.

5.1. Counter-flow experiments

Wong et al. (2010) provide a set of 89 controlled experiments in which two pedestrian groups of varying size intersect at different angles. These experiments were carried out in a sports hall in Hong Kong, and video footage is available. Among the set of experiments,

those with high densities and an intersection angle of 180° yield the highest level of anisotropy (Wong et al., 2010). Table 1 provides a list of the corresponding experiments, and Fig. 2 describes the 3 m wide and 9 m long walking corridor for the controlled experiments.

(a) Sample image extracted from experiment #85

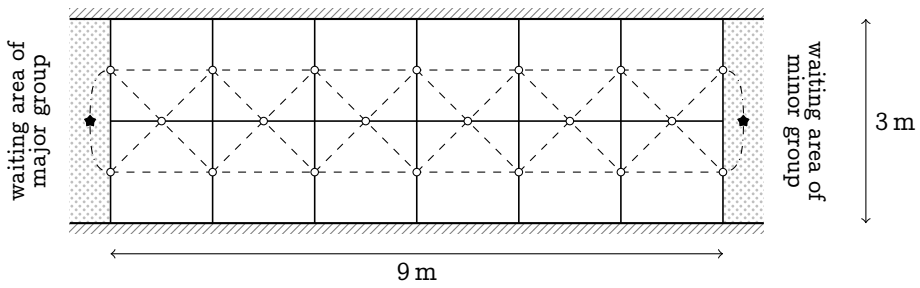

(b) Walkway configuration

Figure 2: Experimental setup of counter-flow experiments (Wong et al., 2010).

Table 1: Observed walking speeds in counter-flow experiments.

Exp.	major group		minor group	
#84	87 ped	1.08 ± 0.15 m/s	–	–
#85	79	1.19 ± 0.13	9 ped	0.80 ± 0.14 m/s
#86	68	0.90 ± 0.10	18	0.74 ± 0.15
#87	61	0.82 ± 0.06	26	0.67 ± 0.10
#88	53	0.83 ± 0.09	30	0.79 ± 0.15
#89	44	0.79 ± 0.10	44	0.79 ± 0.18

Each experiment is conducted once and lasts about 1 min. Pedestrians associated with the major group wear blue hats, and those associated with the minor group wear green hats. Due to a flat viewing angle and high density, no automatic data processing is feasible. Instead, we have manually extracted the departure and walking time of each pedestrian in the six experiments of interest. The ratio of the pedestrian group sizes varies from approximately 10:0, 9:1, 8:2, 7:3, 6:4 to 5:5, of which the first and last

experiment yield isotropic flows.

To evaluate the proposed model specifications, they are calibrated on two experiments, and cross-validated on the remaining ones. We have tested different compositions and sizes of the training and validation sets, but the results do not change significantly. Importantly, the training set should contain experiments with anisotropic walking behavior. In the following, experiments #85 and #87 are used for calibration, and experiments #84, 86, 88 and 89 for validation. Table 2 shows the obtained parameter values and the corresponding AIC values for four different density-speed relationships. The number of observations available for each experiment corresponds to the number of pedestrians involved, and is indicated in brackets. The number of estimation parameters is two, three, four and four for the Zero-, Drake-, Weidmann and SbFD-model, respectively.

Table 2: Results of calibration and validation on counter-flow experiments.

	Zero-Model	Drake	SbFD	Weidmann
$AIC^{calib}_{85,87}$ (175 obs.)	837.7	754.0	704.5	729.4
v_f [m/s]	1.166 ± 0.001	**1.170** ± 0.001	**1.115** ± 0.000	1.169 ± 0.001
μ [-]	**1.43** ± 0.06	12.15 ± 0.29	10.18 ± 2.02	14.84 ± 0.30
ϑ [m^4]		**0.078** ± 0.000	**0.001** ± 0.004	
β [m^2]			0.210 ± 0.005	
γ [m^{-2}]				**4.92** ± 0.20
k_{jam} [m^{-2}]				**6.58** ± 0.46
AIC^{valid}_{84} (87 obs.)	355.2	338.4	311.4	348.2
AIC^{valid}_{86} (86 obs.)	381.7	371.3	355.3	401.4
AIC^{valid}_{88} (83 obs.)	400.3	384.6	364.0	435.3
AIC^{valid}_{89} (88 obs.)	458.2	408.8	396.8	454.6

The stream-based pedestrian fundamental diagram (SbFD) reaches a better AIC value than the two other fundamental diagrams (Weidmann, Drake), both as far as the training set and the validation experiments are concerned. Interestingly, this not only holds for the anisotropic experiments (#86, #88), but also for the uni-directional pedestrian flow experiment (#84) and that with equal flow shares (#89). A look at the mean walking times for the major and minor pedestrian groups in each experiment corroborates that finding (see Table 3). The SbFD-model is able to estimate walking times that are closer to the ones observed, in particular for the minor group. This can also be seen from the significant reduction in the squared error reported at the bottom of Table 3.

In Table 2, the obtained estimates for the free-flow walking speed vary between 1.115 m/s and 1.170 m/s with generally small errors. For the same parameter, Wong et al. (2010) report a value of 1.034 m/s, which is slightly lower. With the exception of the result for the zero-model ($\mu = 1.43$), the values obtained for the path choice parameter μ lie in the range between 10 and 15, which is relatively high as a comparison to the second case study will show. A high value implies that pedestrians tend to stick to the fastest path, which in an experiment like this is expected. A low value on the other hand leads to dispersion, which explains the low estimate obtained by the zero-model. Dispersion is the only way for the zero-model to reproduce a distribution of walking

Table 3: Walking times for counter-flow validation experiments.

Exp.	Groups	tt_{obs} [s]	tt_{Zero} [s]	tt_{Drake} [s]	tt_{SbFD} [s]	$tt_{Weidmann}$ [s]
#84	87 / 0	8.5 / -	9.5 / -	9.1 / -	8.1 / -	8.3 / -
#86	68 / 18	10.1 / **12.7**	9.5 / 9.5	10.0 / 10.8	9.4 / **12.5**	8.8 / 9.5
#88	53 / 31	10.9 / **11.8**	9.5 / 9.5	10.0 / 10.6	10.3 / **11.7**	8.9 / 9.2
#89	44 / 44	11.8 / **11.6**	9.5 / 9.5	11.6 / 11.4	11.7 / **11.6**	9.7 / 9.9
L^2-error (weighted, [s])			21.4 / 23.4	9.0 / 10.5	7.9 / 0.7	22.3 / 23.3

times for a given route, since it does not take into account any density-speed interaction.

The remaining parameters shown in Table 2 are in line with the literature, too. For the Drake-model, the obtained value of ϑ ($0.078\ m^4$) is in good agreement with previous estimates by Wong et al. (2010) and Xie and Wong (2015), reporting $0.075\ m^4$ and $0.065\ m^4$, respectively. The same parameter estimate for SbFD is significantly lower ($\vartheta = 0.001\ m^4$) since a significant reduction in walking speed at high densities is explained by the friction with opposing pedestrian streams instead. This effect is quantified by the parameter β, for which no comparison to the literature exists. Regarding the Weidmann-specification, the values obtained for the jam density and shape parameter, $k_{jam} = 6.58\ m^{-2}$ and $\gamma = 4.92\ m^{-2}$, are high compared to a European context, for which values of $k_{jam} = 5.4\ m^{-2}$ and $\gamma = 1.913\ m^{-2}$ are reported (Weidmann, 1992). In the Hong Kong experiment, pedestrians are apparently particularly tolerant towards high densities, reducing their walking speed less with increasing density. This is in line with observations from the video footage, and with observations from previous researchers investigating differences in fundamental diagrams across countries (Chattaraj et al., 2009).

5.2. Cross-flow experiment

Plaue et al. (2014) present a multi-directional pedestrian flow experiment conducted in the entrance hall of a university building at TU Berlin, Germany. Unlike in the previous example, pedestrians are not confined to a pre-defined corridor, and not 'conditioned' from foregoing experiments. The observed population consists primarily of students, of which many carry backpacks, musical instruments, or wear heavy winter clothing. The setting is video-recorded using three networked cameras, and trajectories of pedestrians are extracted using a semi-automatic photogrammetric method.

In total, 142 pedestrians traverse the hall from left to right, and 83 pedestrians from top to bottom (see Fig. 3). They intersect at an angle of roughly 90° in a region of about $25\ m^2$. According to Plaue et al. (2014), the maximum density amounts to $5\ ped/m^2$ and the duration of the experiment is 69 s. Fig. 3 shows a sample image of the experimental environment, as well as of the modeling configuration of the walking area concerned. As can be seen from Fig. 3b, the various entrance and exit zones are modeled by six origin/destination nodes. Local obstacles, namely the two supporting columns, are considered by an according reduction of the surface size of the affected areas.

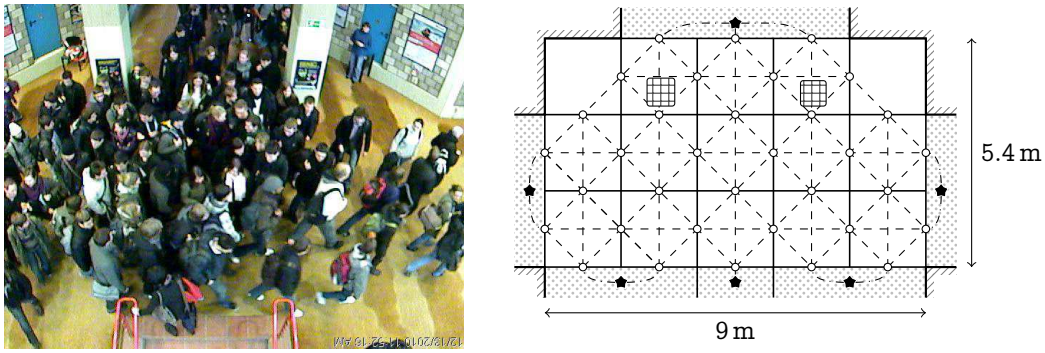

(a) Sample image (b) Area configuration

Figure 3: Setting of cross-flow experiment at TU Berlin (Plaue et al., 2014).

The various model parameters are calibrated on the full data set (see Table 4). The number of observations corresponds to 225 measurements of walking times. Considering the decrease in the AIC value as compared to the zero-model, all 'non-trivial' fundamental diagrams represent improvements, with the anisotropic SbFD having the lowest AIC value overall.

Table 4: Results of calibration on cross-flow experiment.

	Zero-Model	Drake	SbFD	Weidmann
AIC	1160.0	1101.0	1062.6	1098.8
v_f [m/s]	**1.307** ± 0.005	1.308 ± 0.001	1.308 ± 0.006	**1.332** ± 0.002
μ [-]	**1.16** ± 0.03	1.39 ± 0.02	**2.64** ± 0.41	2.05 ± 0.20
ϑ [m^4]		0.139 ± 0.004	0.143 ± 0.004	
β [m^2]			0.300 ± 0.008	
γ [m^{-2}]				1.76 ± 0.15
k_{jam} [m^{-2}]				5.99 ± 0.61

The parameter estimates shown in Table 4 are in agreement with intuitive expectations. The free-flow walking speeds are estimated between 1.307 m/s and 1.332 m/s, which is similar to previous studies from Europe (e.g. 1.34 m/s according to Weidmann, 1992). The path choice parameter lies in the range between 1.16 and 2.64, which is significantly lower than that in the Hong Kong experiments. Pedestrians seem more willing to deviate from the fastest path, for instance to avoid zones of high density. The entrance hall at TU Berlin leaves more room for such deviations than the narrow corridor used in the Hong Kong experiments. The values obtained for the remaining parameters are comparable to the ones found in the previous case study. The sensitivity to density is however larger, as can be seen from the higher values of ϑ and β, as well as the lower values of γ and k_{jam}. Besides differences in the experimental conditions, this is likely

due to the larger physique of Europeans and their lower tolerance to invasion of space (Lam et al., 2002).

Of all parameters, the path choice parameter μ has the largest relative standard deviation from the mean, referred to as the coefficient of variation (CoV). For SbFD, the CoV of μ corresponds to 15.6%. In turn, the relative standard deviation of the free-flow walking speed v_f is the lowest with a CoV of 0.5%. This is in agreement with our experience, according to which identifying the optimal value of v_f is relatively easy, whereas the calibration of μ takes more computational time. It is likely that a more realistic specification of the en-route path choice model, or the use of other data than walking times would improve its identifiability.

A further way to validate the estimation results is with the observed walking times. Fig. 4 provides a scatter plot, comparing the observed walking time of pedestrian i, tt_i^{obs}, to the estimated walking time distribution of the corresponding pedestrian packet $\ell(i)$, as approximated by the mean $\overline{tt}^{est}_{\ell(i)}$ (denoted by circles) and the standard deviation (error bars). For visual guidance, a 45°-reference line (dashed), as well as two isolines (dotted) representing a deviation of $\Delta t = \pm 5$ s are shown. In the figure captions, the squared error is given for each specification.

As expected, the zero-model (Fig. 4a) cannot reproduce the full range of observed walking times, as they are simply proportional to the walked path lengths. This can be seen by the horizontal 'stripes' that appear in the scatter plot. Similarly, the Drake-specification (Fig. 4b) predicts walking times that are confined to a relatively narrow band that does not represent the bandwidth observed in reality. The Weidmann-specification (Fig. 4c) is able to reproduce the full width, but with such significant scattering that no improvement in the squared error as compared to the Drake-model is achieved. The SbFD-specification (Fig. 4d) finally is able to reproduce the observed width, and the squared error is significantly reduced. The spreading is narrower than that for Weidmann, and the estimated walking time distributions come to lie closer to the 45°-reference line. Nevertheless, the remaining scatter is still substantial. The observed stochasticity is likely due to individual differences in walking behavior in presence of congestion, ranging from a pro-active 'sneaking through' to a more passive 'waiting for a gap,' which may cause a large prediction uncertainty.

Table 5: Aggregate route walking times for Berlin case study.

	n_{ped}	tt_{obs} [s]	tt_{Zero} [s]	$tt_{Weidmann}$ [s]	tt_{Drake} [s]	tt_{SbFD} [s]
W → E (9 m)	118	**12.4** (base)	10.8 (-12.7%)	14.0 (+12.6%)	13.3 (+7.2%)	**12.6 (+1.8%)**
N → SE/SW (7 m)	46	**10.6** (base)	8.4 (-21.3%)	9.9 (-6.8%)	10.0 (-6.2%)	**10.9 (+2.2%)**

In relation to these scatter plots, Table 5 summarizes both the observed and estimated aggregate walking times for the two most frequently used routes. Route 'W → E' (left to right) carries the major pedestrian flow, and has a length of 9 m. Route 'N → SE/SW' (top to lateral nodes at the bottom) carries the minor pedestrian flow, and is approximately 7 m long. The observed average walking speed of the major stream amounts

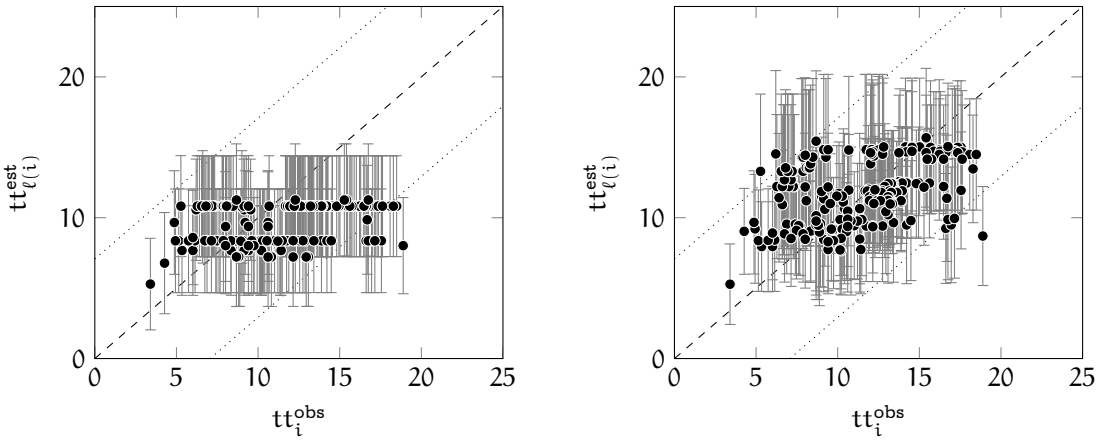

(a) Zero-Model (L^2-error: 53.3 s)

(b) Drake (L^2-error: 47.6 s)

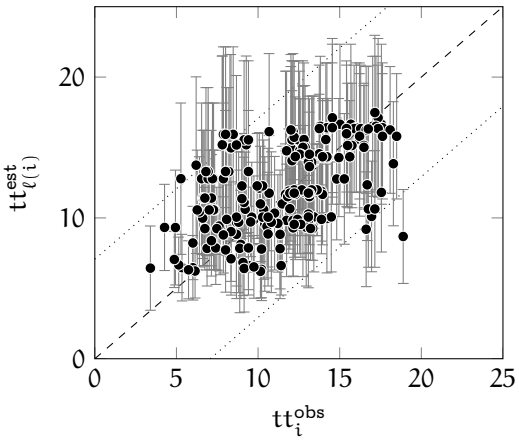

(c) Weidmann (L^2-error: 47.4 s)

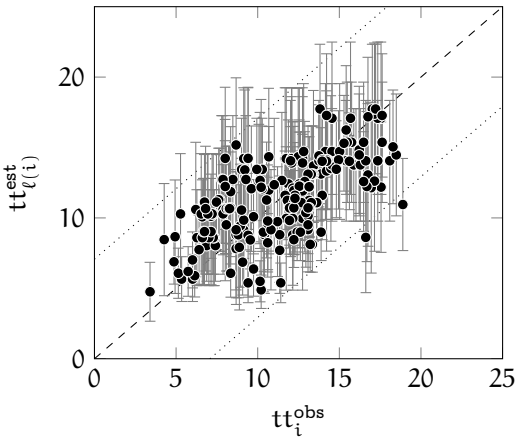

(d) SbFD (L^2-error: 39.2 s)

Figure 4: Scatter plot of walking times for Berlin case study.

to 0.72 m/s (= 9 m/12.4 s), whereas for the minor stream a walking speed of 0.66 m/s (= 7 m/10.6 s) is observed, i.e., anisotropy is clearly present. This anisotropy is not reproduced by neither the Drake- nor the Weidmann-based specification, which both overestimate the walking time of the major stream, and underestimate the walking time of the minor stream. The stream-based fundamental diagram (SbFD), however, yields walking time estimates with errors of 1.8% and 2.2% only. This shows that the explicit consideration of anisotropy for estimating the walking times is not only highly beneficial at the disaggregate, but also at the aggregate level.

6. Discussion

The two investigated case studies unanimously show that the anisotropic specification of the proposed pedestrian network loading model is superior to those based on Weidmann's or Drake's fundamental diagram. This finding holds throughout the analysis and is based on the Akaike information criterion, which takes the number of parameters into account. The Hong Kong counter-flow experiments underline the importance of the stream density ratio when studying walking speeds in congested, multi-directional flow. The Berlin case study considers a cross-flow situation, where random variations in flow direction are present due to pedestrians avoiding areas of high density, obstacles, or those overtaking others. The two case studies together are representative in that they cover both a large range of pedestrian traffic conditions and real-world flows in a challenging environment. In each case, the SbFD-specification shows the best performance both in the calibration and validation.

The calibrated model parameters are in good agreement with the literature. The values of free-flow speed obtained for the Berlin case study are slightly higher than for the Hong Kong case study. For instance, in case of the SbFD-specification, they amount to 1.308 m/s and 1.115 m/s, respectively. Inversely, the jam density is lower in the Berlin than in the Hong Kong case study, with values of 5.99 ped/m^2 and 6.58 ped/m^2. All shape parameters indicate a stronger sensitivity of walking speed with respect to pedestrian density in the Berlin case study. These differences can be explained by regional differences between Europe and Asia (Lam et al., 2002; Chattaraj et al., 2009). Besides, the tightly controlled experimental conditions in the Hong Kong experiments lead to a route choice behavior that is mainly characterized by the pursuit of the shortest path. In the Berlin case study, pedestrians tend to deviate more from the shortest path. The resulting values of the en-route path choice parameter μ reflect that behavior.

The successful calibration of both the fundamental diagrams and the en-route path choice model is particularly encouraging since only the pedestrian demand and walking times are required, while typically their estimation necessitates measurements of density and speed. For the calibration of multi-directional fundamental diagrams, usually even trajectory data is required, which is expensive to collect.

A central strength of the proposed model is its computational performance. On a standard desktop machine, the anisotropic pedestrian flows occurring in the Berlin case study can be computed for a given parameter set in about one second, which is almost 100 times faster than real-time. In contrast, commercial microscopic simulators operate typically at the speed of real-time only.

The small number of parameters, and the direct physical interpretation they allow for, facilitate their transferability from one case study to another. If the proposed model is to be used for a practical application without further calibration, we suggest to use the parametrization obtained from the Berlin case study, whose experimental conditions are particularly realistic. The corresponding specification of the stream-based pedestrian fundamental diagram is illustrated by Fig. 5.

The contour plot shows the expected walking speeds in a counter-flow scenario for various total densities (represented by the x-axis), and different stream density ratios

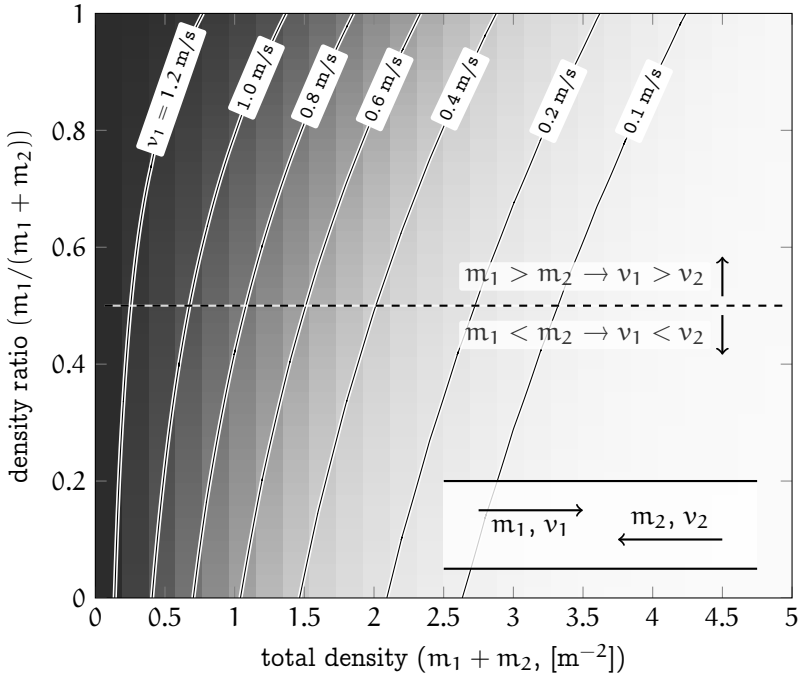

Figure 5: Walking speed for bi-directional flow (SbFD, Berlin data).

(y-axis). Due to the symmetry of the problem, only the speed of one stream is shown. At low densities, the difference in speed between the two opposing streams is relatively small, independently of the stream density ratio. The prevalent speeds are close to the free-flow speed. At high total densities (≥ 1.5 ped/m^2), the prevalent speed of the major stream can be several times higher than that of the minor stream, and speeds are in general lower.

A limitation of the model is due to its exclusive consideration of macroscopic walking, ignoring other activities such as waiting or phenomena involving social interaction between individuals. For instance, group walking patterns are known to significantly influence crowd dynamics (Moussaïd et al., 2010). Similarly, non-walking facility elements such as turnstiles or stairs cannot be described by the model.

A further criticism may relate to the fact that phenomena of self-organization are not reproduced by the proposed model specification. The spontaneous formation of lanes in counter-flow, or of stripes in cross-flow, is indeed well known, both empirically (Helbing et al., 2001) and from modeling (Helbing and Molnár, 1995; Treuille et al., 2006; Hoogendoorn et al., 2014). The question of whether macroscopic models should be able to reproduce such patterns is however debatable. First, it may be argued that empirically calibrated fundamental diagrams already capture the influence of self-organization implicitly (Zhang et al., 2012). Second, most macroscopic models are deterministic, whereas self-organized flow patterns emerge spontaneously, and can hardly be predicted.

For instance, even for homogenous counter-flow in a simple corridor, the configuration and position of lanes change over time, such that on average no lanes may be discernible. Not predicting any spontaneous patterns of self-organization, and accounting for their impact on flow implicitly, may thus be preferable in a deterministic modeling context.

Overall, the proposed model seems highly useful for the planning and design of congested walking facilities. Typically, the assessment of pedestrian infrastructures is based on aggregate quantities such as density and specific flow (Fruin, 1971; Highway Capacity Manual, 2000). Such information is readily available from the model, allowing a quantitative prediction of the expected level-of-service in pedestrian facilities (Hänseler et al., 2015a). Due to the performance of the model, a large number of infrastructure configurations and complex walking networks can be evaluated in little time. Even an automated optimization may be considered, using for instance an evolutionary framework to 'streamline' the design of a facility (Helbing et al., 2002).

7. Conclusions

A dynamic network loading model for congested, multi-directional and time-varying pedestrian flows has been presented. Its novelty lies in the explicit consideration of anisotropy within a macroscopic framework, which is achieved by using a 'stream-based' fundamental diagram for pedestrian traffic. To assess the performance of the proposed model, several isotropic and anisotropic specifications are considered, and evaluated at the example of two case studies. The first considers a set of pedestrian counter-flow experiments in Hong Kong, covering a particularly large range of experimental conditions. The second case study focuses on a pedestrian cross-flow experiment in Berlin, involving students in a university environment. A detailed analysis shows that the consideration of anisotropy significantly improves the accuracy of the proposed model, and that a stream-based pedestrian fundamental diagram outperforms all of the tested isotropic specifications. The obtained specifications of pedestrian fundamental diagrams are in excellent agreement with the literature.

In the future, the proposed model may be improved by developing specifications that capture anisotropy in more detail. Besides, its application for OD demand estimation or for crowd management seems interesting, as it is one of very few models that allow to generate reproducible and accurate walking time distributions in a single run and at low cost.

Acknowledgements

We thank J.M. Fonseca, M. de Lapparent and R. Scarinci (all EPFL), S.P. Hoogendoorn (TU Delft), U. Weidmann (ETH Zürich) and two anonymous referees for their valuable comments. We thank S.C. Wong (The University of Hong Kong) and M. Plaue (TU Berlin) for making available their experimental data. Help by J.-P. Lebacque (IFSTTAR) in the theoretical understanding of the Godunov scheme is appreciated. This work is jointly supported by research grants from the Swiss National Science Foundation (SNSF grant #200021–141099), the Research Committee of the Hong Kong Polytechnic

University for the in-bound PhD student exchange program, and the Research Grants Council of the Hong Kong Special Administrative Region, China (Project No. PolyU 5243/13E).

Appendix A. Numerical scheme

Since pedestrian streams are uni-directional, the associated flow is given by the hydrodynamic theory as the product of speed and density. Specifically, for stream $\lambda \in \Lambda_\xi$ during time interval τ, the flow increment during an infinitesimal time interval dt can be expressed as

$$dQ_{\lambda,\tau} = \frac{M_{\lambda,\tau}}{L_\lambda} v_f F_{\lambda,\tau}(\mathbf{M}_{\xi,\tau}) dt. \tag{A.1}$$

Based on Eq. (7), and by defining the minimum stream length as $L_{min} = \min_{\lambda\in\Lambda} L_\lambda$, the cumulative hydrodynamic flow of stream λ during time interval τ is given by

$$\Delta Q_{\lambda,\tau} = \frac{L_{min}}{L_\lambda} M_{\lambda,\tau} F_{\lambda,\tau}(\mathbf{M}_{\xi,\tau}). \tag{A.2}$$

The cumulative hydrodynamic stream flow does not represent an actual flow, but is a characteristic quantity from which further stream properties can be calculated (Daganzo, 1994).

Due to properties (2) and (3), the function defined in Eq. (A.2) is known to reach a maximum $\Delta Q^{crit}_{\lambda,\tau}$ at a characteristic accumulation $M^{crit}_{\lambda,\tau}$, referred to as the critical cumulative hydrodynamic flow and the critical stream accumulation, respectively. For each stream and time interval, the critical accumulation $M^{crit}_{\lambda,\tau}$ divides the density-flow relationship (Eq. A.2) into a free-flow and a congested regime. In the free-flow regime, an infinitesimal increase in accumulation leads to an increased cumulative hydrodynamic flow. In the congested regime, inversely an increase in accumulation leads to a decrease in pedestrian flow.

The critical accumulation associated with stream λ during time interval τ is computed by assuming that the accumulation of all other pedestrian streams in the same area, $\mathbf{M}'_{\xi,\tau}$ with $\lambda' \in \Lambda_\xi$ and $\lambda' \neq \lambda$, are known, i.e.,

$$M^{crit}_{\lambda,\tau} = \arg\max_{M\geq 0} M F_{\lambda,\tau}(M; \mathbf{M}'_{\xi,\tau}). \tag{A.3}$$

If the critical walking speed of stream λ during time interval τ is given by $v^{crit}_{\lambda,\tau} = v_f F_{\lambda,\tau}(M^{crit}_{\lambda,\tau}; \mathbf{M}'_{\xi,\tau})$, the critical cumulative hydrodynamic flow of stream λ during time interval τ is given by

$$\Delta Q^{crit}_{\lambda,\tau} = \frac{L_{min}}{L_\lambda} M^{crit}_{\lambda,\tau} \frac{v^{crit}_{\lambda,\tau}}{v_f}. \tag{A.4}$$

The cumulative hydrodynamic flow allows to determine an outflow capacity at the end of a stream, and an inflow capacity at the beginning (Lebacque, 1996). The hydrodynamic outflow capacity can be thought of as the maximum amount of pedestrians that could be sent to a next stream in case of an unlimited supply. It is defined as equal

to the cumulative hydrodynamic flow if the stream is in the free-flow regime, and set equal to the critical cumulative hydrodynamic flow if it is in the congested regime. The hydrodynamic outflow capacity of stream λ during time interval τ is thus given by

$$\Delta Q^{\text{out}}_{\lambda,\tau} = \begin{cases} \Delta Q_{\lambda,\tau} & \text{if } M_{\lambda,\tau} \leq M^{\text{crit}}_{\lambda,\tau}, \\ \Delta Q^{\text{crit}}_{\lambda,\tau} & \text{otherwise.} \end{cases} \tag{A.5}$$

Likewise, the hydrodynamic inflow capacity can be considered as the maximum amount of pedestrians that can be received by a stream in case of an infinite traffic demand. It is equal to the critical cumulative hydrodynamic flow if the stream is in the free-flow regime, and set equal to the cumulative hydrodynamic flow otherwise. This is, the cumulative hydrodynamic inflow capacity of stream λ' during time interval τ is given by

$$\Delta Q^{\text{in}}_{\lambda',\tau} = \begin{cases} \Delta Q^{\text{crit}}_{\lambda',\tau} & \text{if } M_{\lambda',\tau} \leq M^{\text{crit}}_{\lambda',\tau}, \\ \Delta Q_{\lambda',\tau} & \text{otherwise.} \end{cases} \tag{A.6}$$

Eq. (A.5) and Eq. (A.6) are similar as in the cell transmission model (Daganzo, 1994), but defined at the stream- instead of the area-level.

The cumulative hydrodynamic inflow and outflow capacity are used to define the receiving and sending capacity, respectively. The receiving capacity of stream λ' during time interval τ is equal to the cumulative hydrodynamic inflow capacity

$$R_{\lambda',\tau} = \Delta Q^{\text{in}}_{\lambda',\tau}, \tag{A.7}$$

where a separate variable is defined for notational consistency with the original CTM. Different from the original CTM, the receiving capacity does not take the area storage capacity N^{jam}_{ξ} into account. Instead, the storage capacity is considered at the area level as described below.

The counterpart of the receiving capacity is the sending capacity. The sending capacity from stream λ to stream $\lambda' \in \Theta^{\rho}_{\lambda}$ for pedestrian packet ℓ during time interval τ is given by

$$S^{\ell}_{\lambda\to\lambda',\tau} = \delta^{\rho_\ell}_{\lambda\to\lambda',\tau} \min\left\{ M^{\ell}_{\lambda,\tau}, \frac{M^{\ell}_{\lambda,\tau}}{M_{\lambda,\tau}} \Delta Q^{\text{out}}_{\lambda,\tau} \right\}. \tag{A.8}$$

The first term in the curly brackets ensures the conservation of pedestrian flow, i.e., not more pedestrians may advance than are actually on the emitting stream. The second term applies when the hydrodynamic outflow capacity does not suffice to advance all pedestrians present on the stream concerned. In that case, a demand-proportional supply distribution scheme is applied to determine the fraction of each pedestrian fragment that is part of the sending capacity.

If the sending capacities exceed the available receiving capacity, they can only be accommodated partially. Let the candidate inflow to stream λ' during time interval τ be given by

$$S_{\lambda',\tau} = \sum_{\lambda''\in\Phi^{\rho}_{\lambda'}} \sum_{\ell\in\mathcal{L}} S^{\ell}_{\lambda''\to\lambda',\tau}, \tag{A.9}$$

where $\Phi^{\rho}_{\lambda'}$ is the set of streams that terminate at the start node of stream λ' and are part of route ρ.

Taking the constraints at the stream level into account, the candidate transition flow from stream λ to λ' during time interval τ associated with pedestrian packet ℓ is expressed as

$$Y^{\ell}_{\lambda\to\lambda',\tau} = \begin{cases} S^{\ell}_{\lambda\to\lambda',\tau} & \text{if } S_{\lambda',\tau} \leq R_{\lambda',\tau}, \\ \zeta^{\ell}_{\lambda\to\lambda',\tau} R_{\lambda',\tau} & \text{otherwise.} \end{cases} \tag{A.10}$$

If the candidate inflow to stream λ' is inferior or equal to the corresponding receiving capacity, the candidate transition flow is equal to the sending capacity. Otherwise, the flow disperses and a demand-proportional supply distribution scheme is applied, i.e.,

$$\zeta^{\ell}_{\lambda\to\lambda',\tau} = \frac{S^{\ell}_{\lambda\to\lambda',\tau}}{S_{\lambda',\tau}}. \tag{A.11}$$

Finally, besides constraints at the stream level, also a storage constraint at the area level should be considered if a jam density has been defined. Let the candidate inflow to area ξ' during time interval τ be given by

$$Y_{\xi',\tau} = \sum_{\lambda'\in\Lambda_{\xi'}} \sum_{\lambda''\in\Phi_{\lambda'}} \sum_{\ell\in\mathcal{L}} Y^{\ell}_{\lambda''\to\lambda',\tau}. \tag{A.12}$$

The actual transition flow from stream λ to $\lambda' \in \Lambda_{\xi'}$ during time interval τ associated with pedestrian packet ℓ can then be expressed as

$$G^{\ell}_{\lambda\to\lambda',\tau} = \begin{cases} Y^{\ell}_{\lambda\to\lambda',\tau} & \text{if } Y_{\xi',\tau} \leq N^{\text{jam}}_{\xi'} - N_{\xi',\tau}, \\ \eta^{\ell}_{\lambda\to\lambda',\tau}\left(N^{\text{jam}}_{\xi'} - N_{\xi',\tau}\right) & \text{otherwise.} \end{cases} \tag{A.13}$$

If the residual storage capacity at the area level is sufficient, all candidate transition flows are accommodated. Otherwise, a demand-proportional supply distribution is applied, i.e.,

$$\eta^{\ell}_{\lambda\to\lambda',\tau} = \frac{Y^{\ell}_{\lambda\to\lambda',\tau}}{Y_{\xi',\tau}}. \tag{A.14}$$

If there is no storage capacity at the area level, it holds $N^{\text{jam}}_{\xi} \to \infty$, and thus $G^{\ell}_{\lambda\to\lambda',\tau} \equiv Y^{\ell}_{\lambda\to\lambda',\tau}$. This is the case for the large class of fundamental diagrams that do not define a jam density (see Nikolić et al., 2016, for an overview).

For streams adjacent to origin/destination nodes, source and sink terms need to be included. The generation term for stream $\lambda : \nu^{\lambda}_{o} \to \nu^{\lambda}_{d}$ during time interval τ associated with pedestrian packet ℓ is expressed as

$$W^{\ell}_{\lambda,\tau} = \begin{cases} X_{\ell} & \text{if } \nu^{\lambda}_{o} = \nu^{\rho_\ell}_{o},\ \tau = \tau_{\ell}, \\ -M^{\ell}_{\lambda,\tau} & \text{if } \nu^{\lambda}_{d} = \nu^{\rho_\ell}_{d}, \\ 0 & \text{otherwise.} \end{cases} \tag{A.15}$$

Source/sink areas are assumed to have infinite capacity. Newly added pedestrians that are unable to advance to a next stream are retained in their origin area until the pedestrian traffic situation allows them to do so. Pedestrians reaching their destination are

immediately cleared out. If an exit capacity needs to be considered, this may be done by interposing an area with a corresponding static capacity.

Once the transition flows and generation terms defined in Eq. (A.13) and Eq. (A.15) are known, a flow balance equation allows to update the accumulation of each pedestrian packet in every stream using the difference scheme

$$M^{\ell}_{\lambda,\tau+1} = M^{\ell}_{\lambda,\tau} + \sum_{\lambda' \in \Phi^{\rho\,\ell}_{\lambda}} G^{\ell}_{\lambda' \to \lambda,\tau} - \sum_{\lambda'' \in \Theta^{\rho\,\ell}_{\lambda}} G^{\ell}_{\lambda \to \lambda'',\tau} + W^{\ell}_{\lambda,\tau}. \tag{A.16}$$

If the demand and the initial state of the system, i.e., the fragment size of all pedestrian packets on all streams at $\tau = 0$, are known, the propagation of pedestrian packets along their routes can be computed by sequentially applying Eq. (A.16) to all packets $\ell \in \mathcal{L}$, streams $\lambda \in \Lambda$ and time intervals $\tau \in \mathcal{T}$.

Recursion (A.16) is independent of the processing order within a time interval, i.e., the order in which streams are updated does not have an influence on the dynamics of the model. Moreover, Eq. (A.16) guarantees the conservation of each packet and thus represents the discrete counterpart of the continuity equation that is used in fluid dynamics.

Appendix B. Stream-based fundamental diagrams

The stream-based fundamental diagram 'SbFD,' defined by Eq. (8), belongs to a class of density-speed relationships for which the walking speed of pedestrian stream λ can be expressed as

$$v_\lambda = v_f R^{\text{iso}}_{\xi} \prod_{\lambda' \in \Lambda} \exp(-\gamma_{\lambda,\lambda'} k_{\lambda'}). \tag{B.1}$$

In Eq. (B.1), the variable v_f denotes the free-flow walking speed, $R^{\text{iso}}_{\xi} \in [0, 1]$ an isotropic reduction factor, $\gamma_{\lambda,\lambda'}$ a parameter describing the friction of stream λ' on stream λ, and $k_{\lambda'}$ the density of stream λ' (defined as $M_{\lambda'}/A_{\xi'}$ in the loading model, where $A_{\xi'}$ is the size of area ξ' with $\lambda' \in \Lambda_{\xi'}$).

The isotropic reduction factor $R^{\text{iso}}_{\xi}(k_\xi)$ is a function of the area density $k_\xi = \sum_{\lambda \in \Lambda} k_\lambda$. In agreement with the 'monotonicity' assumption stated in Eq. (3), it is required that

$$\frac{\partial R^{\text{iso}}_{\xi}}{\partial k_\xi} \leq 0. \tag{B.2}$$

The parameter $\gamma_{\lambda,\lambda'}$ is assumed to be independent of the densities of streams λ and λ', as well as independent of the properties of any other stream. Typically, $\gamma_{\lambda,\lambda'}$ is a function of the intersection angle $\varphi_{\lambda,\lambda'}$ between streams λ and λ'. It is assumed that the pair-wise friction between parallel streams is zero, i.e.,

$$\gamma_{\lambda,\lambda'} = 0 \text{ if } \varphi_{\lambda,\lambda'} = 0. \tag{B.3}$$

Stream-based fundamental diagrams that can be expressed in the form of Eq. (B.1) and fulfill Eq. (B.3) are 'self-consistent.' This property is illustrated at an example.

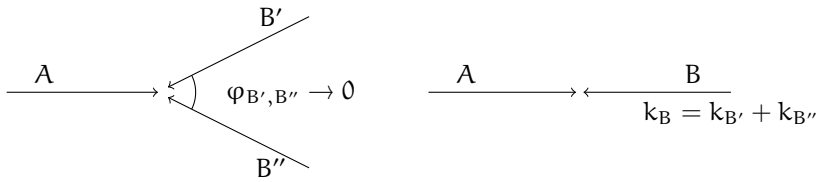

(a) Three streams (b) Two streams

Figure B.6: Illustration of self-consistency.

Consider a stream configuration as shown in Fig. B.6a, where streams A, B′ and B″ with $k_A, k_{B'}, k_{B''} \neq 0$ interact. In the limit case $\varphi_{B',B''} \to 0$, the resulting speeds are equivalent to those obtained for the configuration shown in Fig. B.6b, where the streams B′ and B″ are 'merged' to a single stream B such that $k_B = k_{B'} + k_{B''}$. This can be verified by computing the resulting stream speeds for both configurations. Assuming that $\varphi_{B',B''} = 0$ and $\varphi_{A,B} = \varphi_{A,B'}$, one obtains for stream A

$$v_f R_\xi^{iso} \exp(-\gamma_{A,B'} k_{B'}) \exp(-\gamma_{A,B''} k_{B''}) = v_f R_\xi^{iso} \exp(-\gamma_{A,B} k_B), \tag{B.4}$$

where the LHS corresponds to Fig. B.6a, and the RHS to Fig. B.6b. Eq. (B.4) holds true since $\gamma_{A,B} = \gamma_{A,B'} = \gamma_{A,B''}$ and $k_B = k_{B'} + k_{B''}$. For stream B, one obtains

$$v_f R_\xi^{iso} \exp(-\gamma_{B',A} k_A) \exp(-\gamma_{B',B''} k_{B''}) = v_f R_\xi^{iso} \exp(-\gamma_{B,A} k_A), \tag{B.5}$$

which holds true since $\gamma_{B,A} = \gamma_{B',A}$ and $\gamma_{B',B''} = 0$.

The self-consistency of fundamental diagrams associated with Eq. (B.1) is notably due to the exponential form of the product terms, the linearity of the exponent $(-\gamma_{\lambda,\lambda'} k_{\lambda'})$ in $k_{\lambda'}$, its independence from any other stream densities, and due to the assumed absence of inner friction as expressed by Eq. (B.3). Self-consistency is desirable for theoretical reasons, but also to avoid a recalibration of the model in case parallel streams are merged (see Fig. B.6). Particular emphasis is given to that property as already in the Berlin case study multiple parallel streams are present (see diagonal streams in Fig. 3b). If only a small number of streams with distinct angles are considered, self-consistency may be less relevant. For instance, the specifications provided by Wong et al. (2010) and Xie and Wong (2015) cannot be cast in the form of Eq. (B.1).

The SbFD defined in Eq. (8) results from Eq. (B.1) by setting $R_\xi^{iso} = \exp(-\vartheta k_\xi^2)$ as well as $\gamma_{\lambda,\lambda'} = \beta(1 - \cos(\varphi_{\lambda,\lambda'}))$. We have tested several specifications of the isotropic reduction term R_ξ^{iso}, including those proposed by Tregenza (1976) and Weidmann (1992), as well as a linear specification (Older, 1968; Navin and Wheeler, 1969). This set of specifications is motivated by the findings of Nikolić et al. (2016). An analysis based on the case studies discussed in Section 5 shows that the Drake-model performs best (Fonseca, 2015). This is in line with the results by Wong et al. (2010) and Xie and Wong (2015), who also use the Drake-model to specify the isotropic reduction term.

Likewise, we have examined several specifications of the parameter $\gamma_{\lambda,\lambda'}$ that describes the dependency of the pair-wise stream friction on the intersection angle $\varphi_{\lambda,\lambda'}$. A comparison with a linear and a piecewise linear model shows that the chosen trigonometric specification yields the best performance, at least as far as the AIC and BIC are concerned. The specification $\gamma_{\lambda,\lambda'} = \beta(1 - \cos(\varphi_{\lambda,\lambda'}))$ naturally respects Eq. (B.3), and it is symmetric with respect to the 180°-plane and 360°-periodic. It implies that the friction between streams is maximal for head-on flow, and that the friction grows most rapidly at an intersection angle of $\varphi = 90°$, i.e., when the behavioral regime changes from 'leader-follower' to 'collision avoidance' (Bierlaire and Robin, 2009). Within each of these behavioral regimes, the friction still grows with an increasing intersection angle, but not as much as at the transitional angle $\varphi = 90°$, where the slope amounts to $d\gamma/d\varphi = \beta$. Wong et al. (2010) propose the same relationship to describe the γ–φ-dependency, whereas Xie and Wong (2015) consider a specification that is not symmetric with respect to the 180°-plane.

References

Abdelghany, A., Abdelghany, K., Mahmassani, H. S., Al-Zahrani, A., 2012. Dynamic simulation assignment model for pedestrian movements in crowded networks. Transportation Research Record: Journal of the Transportation Research Board 2316 (1), 95–105.

Al-Gadhi, S. A. H., Mahmassani, H. S., 1990. Modelling crowd behavior and movement: application to Makkah pilgrimage. Transportation and Traffic Theory 1990, 59–78.

Al-Gadhi, S. A. H., Mahmassani, H. S., Herman, R., 2002. A speed-concentration relation for bidirectional crowd movements with strong interaction. Pedestrian and evacuation dynamics, 3–20.

Asano, M., Iryo, T., Kuwahara, M., 2010. Microscopic pedestrian simulation model combined with a tactical model for route choice behaviour. Transportation Research Part C: Emerging Technologies 18 (6), 842–855.

Asano, M., Sumalee, A., Kuwahara, M., Tanaka, S., 2007. Dynamic cell transmission-based pedestrian model with multidirectional flows and strategic route choices. Transportation Research Record: Journal of the Transportation Research Board 2039 (1), 42–49.

Bai, J., 1999. Likelihood ratio tests for multiple structural changes. Journal of Econometrics 91 (2), 299–323.

Bellomo, N., Dogbé, C., 2008. On the modelling crowd dynamics from scaling to hyperbolic macroscopic models. Mathematical Models and Methods in Applied Sciences 18, 1317–1345.

Ben-Akiva, M. E., Lerman, S. R., 1985. Discrete choice analysis: Theory and application to predict travel demand. Vol. 9. MIT Press.

Besag, J., 1975. Statistical analysis of non-lattice data. The statistician, 179–195.

Bierlaire, M., Robin, T., 2009. Pedestrians choices. In: Timmermans, H. J. P. (Ed.), Pedestrian Behavior. Models, Data Collection and Applications. Emerald Group Publishing, Bingley, U.K., pp. 1–26.

Blue, V. J., Adler, J. L., 2001. Cellular automata microsimulation for modeling bi-directional pedestrian walkways. Transportation Research Part B: Methodological 35 (3), 293–312.

Cascetta, E., Inaudi, D., Marquis, G., 1993. Dynamic estimators of origin-destination matrices using traffic counts. Transportation Science 27 (4), 363–373.

Chattaraj, U., Seyfried, A., Chakroborty, P., 2009. Comparison of pedestrian fundamental diagram across cultures. Advances in Complex Systems 12 (03), 393–405.

Chen, M., Bärwolff, G., Schwandt, H., 2014. Modeling pedestrian dynamics on triangular grids. Transportation Research Procedia 2, 327–335.

Colombo, R. M., Garavello, M., Lécureux-Mercier, M., 2012. A class of nonlocal models for pedestrian traffic. Mathematical Models and Methods in Applied Sciences 22 (04), 1150023.

Cooper, G. A., 2014. A multi-class framework for a pedestrian cell transmission model accounting for population heterogeneity. Master's thesis, Ecole Polytechnique Fédérale de Lausanne.

Courant, R., Friedrichs, K., Lewy, H., 1967. On the partial difference equations of mathematical physics. IBM Journal of Research and Development 11 (2), 215–234.
Daganzo, C. F., 1994. The cell transmission model: A dynamic representation of highway traffic consistent with the hydrodynamic theory. Transportation Research Part B: Methodological 28 (4), 269–287.
Daganzo, C. F., 1995. The cell transmission model, Part II: Network traffic. Transportation Research Part B: Methodological 29 (2), 79–93.
Degond, P., Appert-Rolland, C., Pettré, J., Theraulaz, G., 2013. Vision-based macroscopic pedestrian models. Kinetic Related Models 6 (4), 809–839.
Degond, P., Hua, J., 2013. Self-organized hydrodynamics with congestion and path formation in crowds. Journal of Computational Physics 237, 299–319.
Dijkstra, E. W., 1959. A note on two problems in connexion with graphs. Numerische Mathematik 1 (1), 269–271.
Dodge, Y., 2006. The Oxford dictionary of statistical terms. Oxford University Press, Oxford, U.K.
Drake, J. S., Schofer, J. L., May, A. D., 1967. A statistical analysis of speed-density hypotheses. In: Proceedings of the Third International Symposium on the Theory of Traffic Flow. New York, pp. 112–117.
Duives, D. C., Daamen, W., Hoogendoorn, S. P., 2013. State-of-the-art crowd motion simulation models. Transportation Research Part C: Emerging Technologies 37 (12), 193–209.
Fonseca, J. M., 2015. Specification testing of fundamental diagrams for an anisotropic pedestrian network loading model. Bachelor's thesis, Ecole Polytechnique Fédérale de Lausanne.
Fruin, J. J., 1971. Pedestrian planning and design. Metropolitan Association of Urban Designers and Environmental Planners, Michigan, USA.
Gourieroux, C., Monfort, A., Renault, E., 1993. Indirect inference. Journal of Applied Econometrics 8, S85–S85.
Gourieroux, C., Monfort, A., Trognon, A., 1984. Pseudo maximum likelihood methods: Theory. Econometrica: Journal of the Econometric Society, 681–700.
Guo, R. Y., Huang, H. J., Wong, S. C., 2011. Collection, spillback, and dissipation in pedestrian evacuation: A network-based method. Transportation Research Part B: Methodological 45 (3), 490–506.
Hänseler, F. S., 2016. Modeling and estimation of pedestrian flows in train stations. Ph.D. thesis, Ecole Polytechnique Fédérale de Lausanne.
Hänseler, F. S., Bierlaire, M., Farooq, B., Mühlematter, T., 2014. A macroscopic loading model for time-varying pedestrian flows in public walking areas. Transportation Research Part B: Methodological 69, 60–80.
Hänseler, F. S., Bierlaire, M., Scarinci, R., 2015a. Assessing the usage and level-of-service of pedestrian facilities in train stations: A Swiss case study. TRANSP-OR Report Nr. 150108, Ecole Polytechnique Fédérale de Lausanne, Switzerland.
Hänseler, F. S., Lederrey, G., 2015. Java implementation of anisotropic pedestrian loading model. URL `https://github.com/flurinus/AnisoPedCTM`
Hänseler, F. S., Molyneaux, N. A., Bierlaire, M., 2015b. Estimation of pedestrian origin-destination demand in train stations. TRANSP-OR Report Nr. 150703, Ecole Polytechnique Fédérale de Lausanne.
Helbing, D., 1992. A fluid dynamic model for the movement of pedestrians. Complex Systems 6, 391–415.
Helbing, D., Buzna, L., Johansson, A., Werner, T., 2005. Self-organized pedestrian crowd dynamics: experiments, simulations, and design solutions. Transportation Science 39 (1), 1–24.
Helbing, D., Farkas, I., Molnar, P., Vicsek, T., 2002. Simulation of pedestrian crowds in normal and evacuation situations. Pedestrian and evacuation dynamics 21.
Helbing, D., Molnár, P., 1995. Social force model for pedestrian dynamics. Physical Review E 51 (5), 4282–4286.
Helbing, D., Molnar, P., Farkas, I. J., Bolay, K., 2001. Self-organizing pedestrian movement. Environment and Planning B 28 (3), 361–384.
Highway Capacity Manual, 2000. Transportation Research Board. Washington, DC.
Hoogendoorn, S. P., Bovy, P. H. L., 2002. Normative pedestrian behaviour theory and modelling. Transportation and Traffic Theory 15, 219–245.
Hoogendoorn, S. P., Bovy, P. H. L., 2004. Pedestrian route-choice and activity scheduling theory and models. Transportation Research Part B: Methodological 38 (2), 169–190.
Hoogendoorn, S. P., Daamen, W., 2007. Microscopic calibration and validation of pedestrian models: Cross-comparison of models using experimental data. In: Traffic and Granular Flow '05. Springer,

pp. 329–340.
Hoogendoorn, S. P., van Wageningen-Kessels, F., Daamen, W., Duives, D. C., Sarvi, M., 2015. Continuum theory for pedestrian traffic flow: Local route choice modelling and its implications. Transportation Research Part C: Emerging Technologies 59, 183–197.
Hoogendoorn, S. P., van Wageningen-Kessels, F. L. M., Daamen, W., Duives, D. C., 2014. Continuum modelling of pedestrian flows: From microscopic principles to self-organised macroscopic phenomena. Physica A: Statistical Mechanics and its Applications 416, 684–694.
Huang, L., Wong, S. C., Zhang, M., Shu, C. W., Lam, W. H. K., 2009. Revisiting Hughes' dynamic continuum model for pedestrian flow and the development of an efficient solution algorithm. Transportation Research Part B: Methodological 43 (1), 127–141.
Hughes, R. L., 2002. A continuum theory for the flow of pedestrians. Transportation Research Part B: Methodological 36 (6), 507–535.
Jiang, Y., Xiong, T., Wong, S. C., Shu, C. W., Zhang, M., Zhang, P., Lam, W. H. K., 2009. A reactive dynamic continuum user equilibrium model for bi-directional pedestrian flows. Acta Mathematica Scientia 29 (6), 1541–1555.
Jin, W. L., Zhang, H. M., 2003. On the distribution schemes for determining flows through a merge. Transportation Research Part B: Methodological 37 (6), 521–540.
Kirchner, A., Schadschneider, A., 2002. Simulation of evacuation processes using a bionics-inspired cellular automaton model for pedestrian dynamics. Physica A: Statistical Mechanics and its Applications 312 (1), 260–276.
Kretz, T., Grünebohm, A., Kaufman, M., Mazur, F., Schreckenberg, M., 2006. Experimental study of pedestrian counterflow in a corridor. Journal of Statistical Mechanics: Theory and Experiment 2006 (10), P10001.
Lam, W. H. K., Lee, J. Y. S., Cheung, C. Y., 2002. A study of the bi-directional pedestrian flow characteristics at Hong Kong signalized crosswalk facilities. Transportation 29 (2), 169–192.
Lebacque, J.-P., 1996. The Godunov scheme and what it means for first order traffic flow models. In: International Symposium on Transportation and Traffic Theory. pp. 647–677.
Lederrey, G., 2015. A macroscopic loading model for dynamic, anisotropic and congested pedestrian flows: Implementation, calibration and case study analysis. Semester thesis, Ecole Polytechnique Fédérale de Lausanne.
Lighthill, M. J., Whitham, G. B., 1955. On kinematic waves. II. A theory of traffic flow on long crowded roads. Proceedings of the Royal Society of London. Series A. Mathematical and Physical Sciences 229 (1178), 317–345.
Løvås, G. G., 1994. Modeling and simulation of pedestrian traffic flow. Transportation Research Part B: Methodological 28 (6), 429–443.
Moreira, M. J., 2003. A conditional likelihood ratio test for structural models. Econometrica 71 (4), 1027–1048.
Moussaïd, M., Perozo, N., Garnier, S., Helbing, D., Theraulaz, G., 2010. The walking behaviour of pedestrian social groups and its impact on crowd dynamics. PLoS One 5 (4), e10047.
Navin, F. P., Wheeler, R. J., 1969. Pedestrian flow characteristics. Traffic Engineering 39.
Nikolić, M., Bierlaire, M., 2014. Pedestrian-oriented flow characterization. Transportation Research Procedia 2, 359–366.
Nikolić, M., Bierlaire, M., Farooq, B., de Lapparent, M., 2016. Probabilistic speed–density relationship for pedestrian traffic. Transportation Research Part B: Methodological 89, 58–81.
Older, S. J., 1968. Movement of pedestrians on footways in shopping streets. Traffic Engineering & Control 10 (4), 160–163.
Ondřej, J., Pettré, J., Olivier, A.-H., Donikian, S., 2010. A synthetic-vision based steering approach for crowd simulation. In: ACM Transactions on Graphics. Vol. 29. ACM, p. 123.
Piccoli, B., Tosin, A., 2011. Time-evolving measures and macroscopic modeling of pedestrian flow. Archive for Rational Mechanics and Analysis 199 (3), 707–738.
Plaue, M., Bärwolff, G., Schwandt, H., 2014. On measuring pedestrian density and flow fields in dense as well as sparse crowds. In: Pedestrian and Evacuation Dynamics 2012. Springer, pp. 411–424.
Powell, M. J. D., 2009. The BOBYQA algorithm for bound constrained optimization without derivatives. Report DAMTP 2009/NA06, Department of Applied Mathematics and Theoretical Physics, Cambridge University, Cambridge, U.K.
Richards, P. I., 1956. Shock waves on the highway. Operations Research 4 (1), 42–51.

Robin, T., Antonini, G., Bierlaire, M., Cruz, J., 2009. Specification, estimation and validation of a pedestrian walking behavior model. Transportation Research Part B: Methodological 43 (1), 36–56.

Sayir, M. B., Dual, J., Kaufmann, S., 2008. Ingenieurmechanik. Springer.

Schwandt, H., Huth, F., Bärwolff, G., 2013. A macroscopic model for intersecting pedestrian streams with tactical and strategical redirection. In: 11th International Conference of Numerical Analysis and Applied Mathematics. Vol. 1558. AIP Publishing, pp. 2209–2212.

Tregenza, P., 1976. The design of interior circulation. Van Nostrand Reinhold, New York, USA.

Treuille, A., Cooper, S., Popović, Z., 2006. Continuum crowds. In: ACM Transactions on Graphics (TOG). Vol. 25. ACM, pp. 1160–1168.

van Wageningen-Kessels, F., Daamen, W., Hoogendoorn, S., 2015a. The two-dimensional Godunov scheme and what it means for macroscopic pedestrian flow models. Submitted manuscript, Delft University of Technology.

van Wageningen-Kessels, F. L. M., Leclercq, L., Daamen, W., Hoogendoorn, S. P., 2015b. The lagrangian coordinate system and what it means for two-dimensional crowd flow models. Physica A: Statistical Mechanics and its Applications.

Weidmann, U., 1992. Transporttechnik der Fussgänger. Schriftenreihe des IVT Nr. 90. Institute for Transport Planning and Systems, ETH Zürich, Switzerland.

Wong, S. C., Leung, W. L., Chan, S. H., Lam, W. H. K., Yung, N. H. C., Liu, C. Y., Zhang, P., 2010. Bidirectional pedestrian stream model with oblique intersecting angle. Journal of Transportation Engineering 136 (3), 234–242.

Xie, S., Wong, S. C., 2015. A Bayesian inference approach to the development of a multidirectional pedestrian stream model. Transportmetrica A: Transport Science 11 (1), 61–73.

Zhang, J., Klingsch, W., Schadschneider, A., Seyfried, A., 2012. Ordering in bidirectional pedestrian flows and its influence on the fundamental diagram. Journal of Statistical Mechanics: Theory and Experiment 2012 (02), P02002.

Zhang, J., Seyfried, A., 2014. Comparison of intersecting pedestrian flows based on experiments. Physica A: Statistical Mechanics and its Applications 405, 316–325.